Ni stabilised on inorganic complex structures: superior catalysts for chemical CO_2 recycling via dry reforming of methane

E. le Saché[a], L. Pastor-Pérez[a,b], D. Watson[c], A. Sepúlveda-Escribano[b], T.R. Reina[a,*]

[a] Department of Chemical and Process Engineering, University of Surrey, Guildford, GU2 7XH, United Kingdom
[b] Laboratorio de Materiales Avanzados, Departamento de Química Inorgánica - Instituto Universitario de Materiales de Alicante Universidad de Alicante, Apartado 99, E-03080 Alicante, Spain
[c] Department of Chemistry, University of Surrey, Guildford, GU2 7XH, United Kingdom
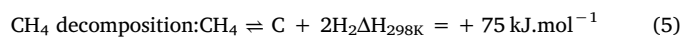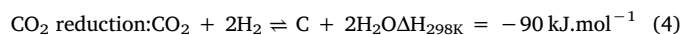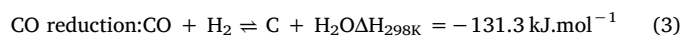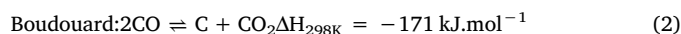
ARTICLE INFO

ABSTRACT

CO_2 utilisation is becoming an appealing topic in catalysis science due to the urgent need to deal with greenhouse gases (GHG) emissions. Herein, the dry reforming of methane (DRM) represents a viable route to convert CO_2 and CH_4 (two of the major GHG) into syngas, a highly valuable intermediate in chemical synthesis. Nickel-based catalysts are economically viable materials for this reaction, however they show inevitable signs of deactivation. In this work stabilisation of Ni in a pyrochlore-perovskite structure is reported as a viable method to prevent fast deactivation. Substitution of Zirconium by Ni at various loadings in the lanthanum zirconate pyrochlore $La_2Zr_2O_7$ is investigated in terms of reactant conversions under various reaction conditions (temperature and space velocity). XRD analysis of the calcined and reduced catalysts showed the formation of crystalline phases corresponding to the pyrochlore structure $La_2Zr_{2-x}Ni_xO_{7-\delta}$ and an additional La_2NiZrO_6 perovskite phase at high Ni loadings. Carbon formation is limited using this formulation strategy and, as a consequence, our best catalyst shows excellent activity for DRM at temperatures as low as 600 °C and displays great stability over 350 h of continuous operation. Exsolution of Ni from the oxide structure, leading to small and well dispersed Ni clusters, could explain the enhanced performance.

1. Introduction

Increasing anthropogenic CO_2 emissions are encouraging extensive research into CO_2 recycling processes. Dry Reforming of Methane (DRM, eq. 1) represents an attractive way to obtain syngas, allowing the conversion of two greenhouse gases into valuable products. Although DRM produces syngas with a low H_2/CO ratio (around 1) compared to other reforming reactions (3 for the steam reforming of methane, 2 for the partial oxidation of methane, 2 for the bi-reforming of methane and from 1 to 2.5 for autothermal reforming) it can be used either to adjust H_2-rich syngas compositions, either in processes that require a carbon monoxide-rich syngas like the hydroformylation synthesis [1]. The Fischer Tropsch synthesis usually requires a H_2/CO syngas mixture of 2 but can benefit from a higher long-chain hydrocarbons selectivity with lower H_2/CO ratios [2]. DRM has been investigated for numerous years and many studies have been conducted on the development of active and coke-resistant catalysts. Conventional catalysts are composed of a metallic active phase dispersed on a support. Typically for DRM, noble metals such as Ru, Rh, Pd and Pt have been found to be very active and coke resistant, but their price and limited availability is shifting

investigation towards transition metals like Ni and Co [2]. Thermodynamically, DRM requires high reaction temperatures to achieve high CH_4/CO_2 conversions but at such temperatures, supported metal catalysts are prone to deactivation due to sintering of the metallic phase [3,4]. Moreover, carbon deposition inevitably occurs due to numerous side reactions such as the Boudouard reaction (eq. 2), CO reduction (eq. 3) and CO_2 reduction (eq. 4), even though not thermodynamically favoured at high temperatures, and CH_4 decomposition (eq. 5) at higher temperatures [5].

$$DRM: CO_2 + CH_4 \leftrightarrow 2CO + 2H_2 \quad \Delta H^o_{298k} = +247\,kJ.mol^{-1} \quad (1)$$

$$Boudouard: 2CO \rightleftharpoons C + CO_2 \quad \Delta H_{298K} = -171\,kJ.mol^{-1} \quad (2)$$

$$CO\ reduction: CO + H_2 \rightleftharpoons C + H_2O \quad \Delta H_{298K} = -131.3\,kJ.mol^{-1} \quad (3)$$

$$CO_2\ reduction: CO_2 + 2H_2 \rightleftharpoons C + 2H_2O \quad \Delta H_{298K} = -90\,kJ.mol^{-1} \quad (4)$$

$$CH_4\ decomposition: CH_4 \rightleftharpoons C + 2H_2 \quad \Delta H_{298K} = +75\,kJ.mol^{-1} \quad (5)$$

Downstream processes typically operate at pressure levels between 20 and 70 bars [1] therefore to reduce the number of costly

compression steps, DRM should be taking place at elevated pressure. Thermodynamically, the deposition of coke becomes more favourable at higher pressures, especially above 10 bars. Hence, high temperatures (above 800 °C) would then be required to balance the loss of conversion induced by pressure.

Thus, for a practical application, there is a need to develop a cost-effective catalyst, able to withstand high temperatures and able to resist deactivation due to coking and sintering. Different strategies have been applied to tackle sintering and carbon deposition over nickel-based catalyst. Boldrin et al. recently summarised these strategies, whose applications can go beyond DRM and could be extended to the development of carbon resistant solid oxide fuel cells anodes [6]. Tuning the acid/base properties of the support, adding promoters to Ni, sulphur passivation and the use of bimetallic formulations have been widely investigated as approaches to enhance the performance of Ni-based catalysts [6–10]. Overall, the metal and promoters used, the nature, redox properties, acid/base features and surface area of the support, the metal particle size, and the interactions between the metal and support are key to obtaining a good activity/stability balance [2,11,12]. Even upon applying these strategies nickel catalysts still show inevitably signs of deactivation [13,14].

An alternative approach is to stabilise the active metal inside the structure of a thermally stable oxide. In doing so, the metal would be immobilised in a structure, thus preventing sintering. The challenge however is for the metal to remain active and accessible in such a structure. Materials such as spinels, perovskites, fluorites, pyrochlores and hexaaluminates have been investigated for DRM and related reforming reactions [1,6,15–21]. Pyrochlores are mixed oxides of general formula $A_2B_2O_7$. The A-site typically represents a large rare-earth tri-valent metal such as La and a tetravalent transition metal of smaller diameter such as Zr occupies the B-site. They are highly crystalline and thermally stable materials with great oxygen mobility [17]. Hence pyrochlores have been used in various reforming reactions. For instance, Wang's group studied $Ni/Ln_2Zr_2O_7$, $Ni/La_2Zr_2O_7$ and $Ni/La_2Sn_2O_7$ for methane steam reforming and emphasized the influence of the A-site and B-site cations on the structure of the pyrochlore and therefore on its catalytic performance [17,18,22]. Kieffer et al. studied the hydrogenation of CO and CO_2 towards methanol using a $Cu/La_2Zr_2O_7$ catalyst and highlighted its coke resistance [23]. These studies were carried out using pyrochlores as a support for the active phase, as they are typically inactive as bulk materials. However, they can become active for reforming when substituting metals in their structure. Weng et al. previously reported the high activity and stability of $La_2Ce_{2-x}Ru_xO_7$ for the autothermal steam reforming of ethanol [24] and $La_2Ce_{2-x}Ni_xO_{7-\delta}$ for the oxidative steam reforming of ethanol [25].

Spivey's group extensively studied the catalytic activity of Rh, Ru, Pt and Ni doped $La_2Zr_2O_7$ pyrochlore catalyst for DRM [26–30]. Small amounts of active metal were substituted in the B-site of the lanthanum zirconate pyrochlore and the noble metal-based catalysts were found to be very active and stable even at low temperature when carbon deposition is favoured. The Ni doped catalyst (1 wt.% Ni) however displayed poor activity and deactivated quickly due to the deposition of polymeric carbon and carbon whiskers [31].

In this scenario, we believe there is a big avenue of research to improve the formulation of Ni-based catalysts stabilised in inorganic structures leading to robust and economically viable catalysts. With the aim of competing with the high activity of noble metal-based pyrochlores, the catalyst structures and compositions were optimised in this work by tuning the Ni loading. The present study focuses on the synthesis, characterisation and catalytic activity of Ni-substituted lanthanum zirconates pyrochlores and pyrochlore-perovskites for DRM. Specifically, 2, 5 and 10 wt.% Ni is substituted on the B-site of the $La_2Zr_2O_7$ pyrochlore, leading to a new generation of highly active and robust catalysts for CO_2 upgrading.

2. Experimental

2.1. Catalysts synthesis

The catalysts were prepared using a modified citrate method described elsewhere [32]. Lanthanum nitrate [$La(NO_3)_3·6H_2O$], nickel nitrate [$Ni(NO_3)_2·6H_2O$], and zirconyl nitrate [$ZrO(NO_3)_2·6H_2O$], provided by Sigma-Aldrich, were used as precursors. The necessary amount of each precursor was dissolved in deionized water and then mixed with a citric acid (CA) solution in the adequate molar ratio of CA:metal as specified elsewhere [31]. The solution was stirred and concentrated in a rotary evaporator. The resulting mixture was allowed to combust on a hot plate and calcined at 1000 °C for 8 h. For simplicity the 0, 2, 5 and 10 wt.% Ni loaded catalysts will henceforth be referred to as LZ, LNZ2, LNZ5 and LNZ10 respectively.

2.2. Catalysts characterisation

The chemical composition of the materials was determined by XRF using an EDAX Eagle III spectrometer with a rhodium source of radiation working at 40 kV.

The textural properties of the supports were characterised by nitrogen adsorption-desorption measurements at −196 °C in an AUTOS-ORB-6 fully automated manometric equipment. The samples were out-gassed under vacuum at 250 °C for 4 h before each measurement. The BET equation was applied to estimate the specific surface area.

X-Ray powder diffraction (XRD) patterns were recorded on a Bruker D8-Advance with a Goebel mirror and a Kristalloflex K 760-80 F X-Ray generation system, fitted with a Cu cathode and a Ni filter. Spectra were registered between 20 and 80 (2θ) with a step size of 0.05° and a time of 3 s per step.

Raman spectroscopy measurements were performed on a Thermo Scientific DXR Raman Microscope using a green laser (λ = 532 nm, maximum power 10 mW) with a spot diameter of 0.7 μm and a pinhole aperture of 50 μm A diffraction grating of 900 grooves mm^{-1}, a CCD detector and a 50× objective were used.

Temperature-programmed reduction (TPR) with H_2 experiments were carried out on the 'as prepared' catalysts in a U-shaped quartz reactor using a 5% H_2/He gas flow of 50 mL min^{-1}, with a heating rate of 10 °C min^{-1}. Samples were treated with flowing He at 150 °C for 1 h before the TPR run. Hydrogen consumption was monitored using an on-line mass spectrometer (Pfeiffer, OmniStar GSD 301).

Temperature-programmed oxidation (TPO) with O_2 experiments were carried out on the spent catalysts in a TGA/SDTA851e/LF/1600 instrument (Mettler Toledo) connected to a mass spectrometer (TGA-MS). Samples were exposed to a 20% O_2/He gas flow from room temperature to 1000 °C, with a heating rate of 10 °C min^{-1}.

TEM images were taken with a JEOL electron microscope (model JEM-2010) working at 200 kV. It was equipped with an INCA Energy TEM 100 analytical system and a SIS MegaView II camera. Samples for analysis were suspended in ethanol and placed on copper grids with a holey-carbon film support.

2.3. Catalytic behaviour

The catalytic behaviour of the prepared catalysts in the dry reforming of methane reaction was evaluated using a fixed bed quartz reactor loaded in an automatized Microactivity Reference apparatus from PID Eng&Tech. The catalysts were sieved and the 100–200 μm fraction were placed in the reactor on a quartz wool bed. Prior to the activity tests, catalysts were reduced *in-situ* under 50 vol.% H_2 in He, at 700 °C during 1 h. The reaction was carried out for 30 h, at atmospheric pressure in the 600–700 °C temperature range, with a reactant feed molar ratio of CH_4:CO_2 = 1:1 in 60 vol.% He. The total flow of reactants was adjusted to achieve Weight Hourly Space Velocity (WHSV) of 15, 30 and 60 L.g^{-1}.h^{-1} which is equivalent to Gas Hourly Space

Table 1
Chemical compositions and physical analysis results for the prepared samples.

Sample	La (wt.%)	Ni (wt.%)	Zr (wt.%)	S_{BET} ($m^2 g^{-1}$)	Pore volume ($cm^3 g^{-1}$) *10^{-3}
LZ	–	–	–	12	42.5
LNZ2	36.5	2.9	39.5	7	19.8
LNZ5	39.7	6.8	32.8	7	15.6
LNZ10	40.3	12.7	24.9	8	19.9

Velocities (GHSV) of 2500, 5000 and 10,000 h^{-1}. Activity tests were performed using 0.100 g of catalyst. The composition of the outlet of the reactor was followed by an online gas chromatography (Agilent Technologies) equipped with two columns (Carboxen-1000 and Porapak-Q) and two detectors (FID and TCD). The carbon balance was closed +-5%.

The conversions (X_i) of the different reactants and products were calculated as follows:

$$X_{CH4}(\%) = 100 * \frac{[CH_4]_{In} - [CH_4]_{Out}}{[CH_4]_{In}}$$

$$X_{CO2}(\%) = 100 * \frac{[CO_2]_{In} - [CO_2]_{Out}}{[CO_2]_{Out}}$$

3. Results and discussion

3.1. Characterisation

The chemical composition and textural properties of the prepared catalysts are listed in Table 1. The metal loading of the prepared samples are close to the intended values of 2, 5 and 10 wt.% Ni respectively. Regarding the textural properties of the samples, the highest surface area and the largest pore volume were displayed by the undoped LZ sample. The introduction of Ni in the formulation of the catalysts led to a slight decrease of the specific surface. The noticeably lower surface area of our samples when compared to conventional supported catalysts (e.g. Ni/Al$_2$O$_3$ with S_{BET} = 164 $m^2.g^{-1}$ [33]) is an important factor to consider and will be discussed with reference to the XRD results. However, high Ni dispersion is achieved despite the low surface area.

To confirm that a A$_2$B$_2$O$_7$ pyrochlore phase has been successfully formed, the freshly calcined materials were analysed using XRD. The resulting patterns are presented in Fig. 1 and all the samples present the

characteristic diffraction features of La$_2$Zr$_2$O$_7$ pyrochlore phase (JCPDS Card No. 01-73-0444). No diffraction peaks of individual La$_2$O$_3$ or ZrO$_2$ phases are observed. The presence of superstructure peaks (331) and (551) proves that the pyrochlore phase was achieved rather than the fluorite phase which is also typical for these materials [34–36]. These two low intensity diffraction peaks, correspond to cation (and anion) ordering in the pyrochlore structure. The substitution of Ni on the B-site did not affect the pyrochlore crystalline structure up to a loading of 5 wt.%. Above 5 wt.% of Ni loading, a separate La$_2$NiZrO$_6$ rhombohedral double perovskite oxide phase is formed, appearing on the XRD with diffraction peaks at 31.5 and 45.1° (JCPDS Card No. 00-044-0624). A small shift in the diffraction peaks towards the lower angles is observed between the doped materials and the pure pyrochlore as emphasized in the inset of Fig. 1. Ni substitution is responsible for an increase in the lattice parameter, provoking this shift. The amount of Ni in the 5 and 10 wt.% samples appears to be above the maximum substitution limit of the pyrochlore structure, resulting in the formation of a separate perovskite phase. This has been reported previously in literature when doping pyrochlores [27,30,37]. In particular, Haynes et al. reported the formation of La$_2$NiZrO$_6$ for 6 wt.% Ni doped La$_2$Zr$_2$O$_7$ when calcined at temperature higher than 900 °C [38]. No peaks attributed to Ni or NiO$_x$ species are observed indicating that Ni is incorporated on the mixed structure and in case some particles are out of the inorganic lattice they are quite small and well dispersed despite the low surface area of these materials.

Considering that the fluorite and pyrochlore structures have the same parent XRD pattern, only differing by the emergence of minor reflections, Raman spectroscopy was used for further analysis of the crystalline structure of the calcined catalysts. Indeed, the X-ray scattering power of rare-earth cations is much more important than the one of oxygen, hence XRD is more sensitive to disorder in the cation sublattice than in the anion sublattice. Raman spectroscopy on the other hand is very sensitive to metal-oxygen vibrational modes [39]. Here the cations are located on the inversion centre and therefore, they do not contribute to the vibrations and only oxide ligands are visible. For this reason, Raman spectroscopy has been widely used as an efficient tool to distinguish defect-fluorite and ordered pyrochlore materials. The group theory predicts six Raman active modes (A$_{1g}$ + E$_g$ + 4 F$_{2g}$) for the pyrochlore structure (Fd3m) and only one Raman mode (F$_{2g}$) for the fluorite structure (Fm3m). In the Raman spectra shown in Fig. 2, all samples present three or more peaks corresponding to the pyrochlore-type structured lanthanum zirconate, in agreement with the XRD results. Four peaks can be distinguished for LZ: one broad Raman peak at
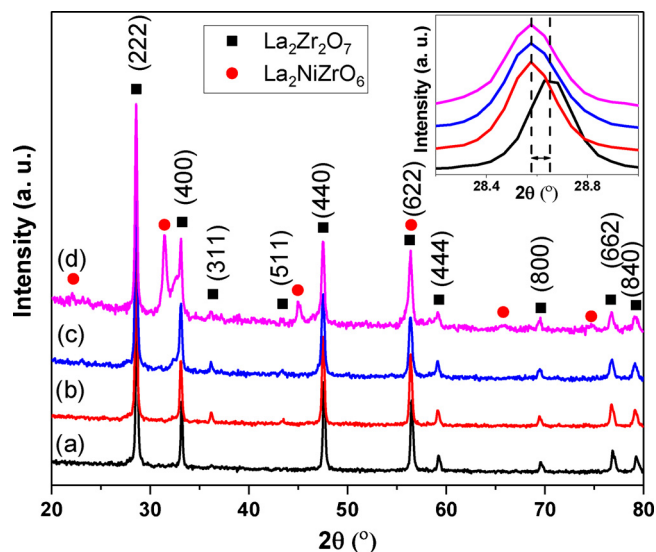

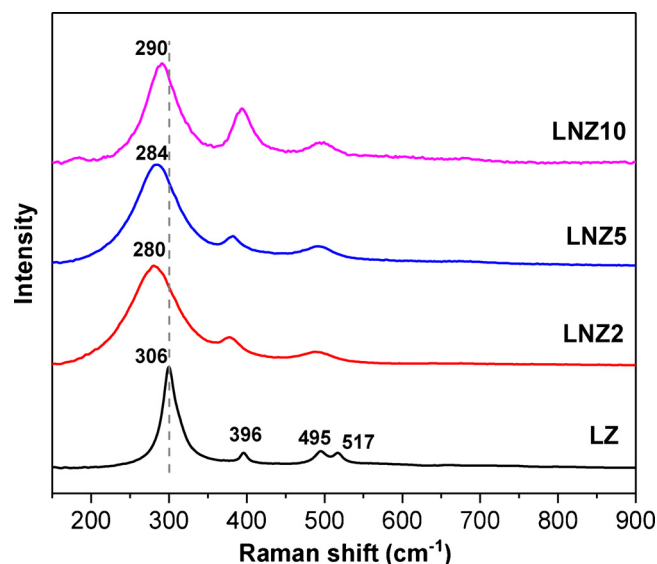**Fig. 1.** XRD pattern of the calcined catalysts (a) LZ, (b) LNZ2, (c) LNZ5 and (d) LNZ10.

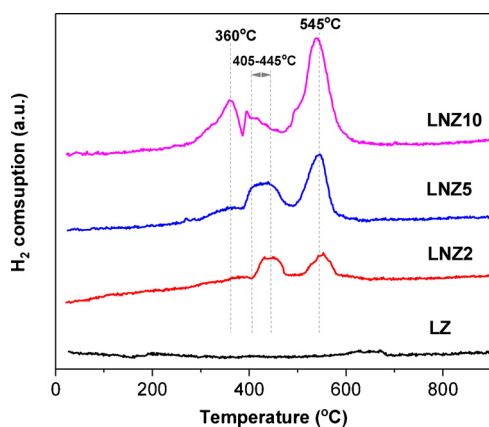**Fig. 2.** Raman spectra of the calcined catalysts LZ, LNZ2, LNZ5 and LNZ10.

Fig. 3. H_2-TPR profiles of the prepared catalysts.

$306\ cm^{-1}$ being the E_g mode associated to O−Zr−O bending vibrations; the A_{1g} mode at $517\ cm^{-1}$ associated to $Zr-O_6$ octahedra bending vibrations and two F_{2g} modes at 495 and $396\ cm^{-1}$ associated to Zr−O and La−O bond stretching with bending vibrations [40–42]. The Raman spectra of the Ni-doped samples evidence in the same way the presence of a pyrochlore structure with the presence of the E_g mode and two F_{2g} modes. A clear shift towards lower wavenumbers is observed between the undoped and the doped materials. The broadening and shift of the doped samples Raman peaks are indicative of an increase in localised disorder across the entire $La_2Zr_2O_7$ structure confirming the incorporation of Ni ions into Zr sites [43].

The reducibility of the four catalysts was studied to determine the conditions needed for the pre-treatment step and to get further insights on their composition and redox properties. The hydrogen TPR profiles of the samples are shown in Fig. 3. The pyrochlore LZ has been found not to be reducible, any H_2 consumption in the doped materials is therefore only due to Ni [17,18]. The profiles of the doped samples depict between two to three peaks. The low temperature peak at 360 °C is attributed to the reduction of NiO located on the surface of the pyrochlore, weakly interacting with it and therefore easily reducible [17]. The medium temperature peaks between 405 and 445 °C are likely to be attributed to Ni exsolved from the pyrochlore structure and interacting with the pyrochlore structure. The most intense peak at 545 °C can be attributed the partial reduction of the La_2NiZrO_6 phase as observed by Haynes et al. [38]. XRD analysis was performed on the reduced samples and the XRD profile of the reduced LNZ10 is shown in Fig. 8. The La_2NiZrO_6 phase is still present indicating that Ni was only partially reduced. Moreover no diffraction peaks due to Ni° are detected indicating that the reduced Ni° particles are small (i.e. under 5 nm) and well dispersed on the surface of the pyrochlore. Therefore, after complete reduction of the catalyst, some Ni is present within the pyrochlore ($La_2Zr_{2-x}Ni_xO_{7-\delta}$) and perovskite ($La_2NiZrO_6$) structures, and also on the surface of the bulk catalyst as small and highly dispersed Ni° nanoparticles.

3.2. Catalytic behaviour

The catalytic behaviour of the catalysts over time on stream at 650 °C is shown in Fig. 4. CO_2 conversion is greater than the CH_4 conversion for all the catalysts. This is due to the higher activation energy of CH_4 (i.e. the energy barrier to activate methane is larger than the one of CO_2 activation) and the occurrence of the Reverse Water Gas Shift (RWGS, eq. 6) reaction, which takes also place under the used conditions. CO_2 reacts with both CH_4 and H_2 resulting in higher CO_2 conversion than expected.

$$RWGS: CO_2 + H_2 \rightleftharpoons CO + H_2O \quad \Delta H_{298K} = +41.2\ kJ/mol \qquad (6)$$
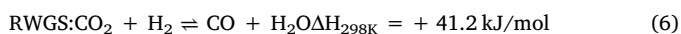
The un-doped LZ pyrochlore does not show any activity in DRM, as

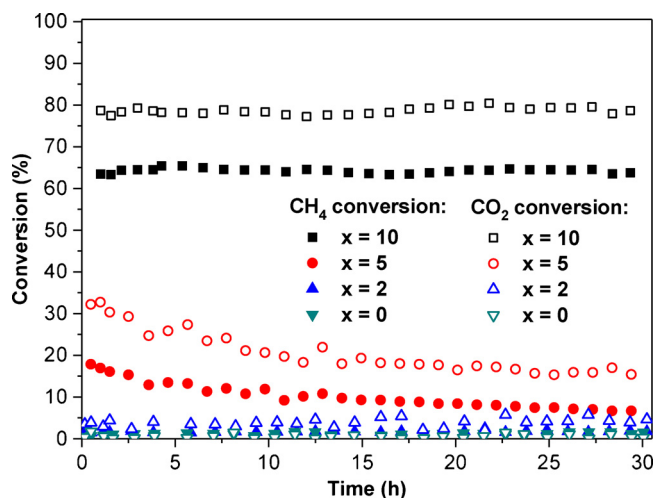**Fig. 4.** Influence of Ni metal loading (x = 0; 2; 5; 10 wt.% Ni) on catalytic activity and stability. Reaction conditions: P = 1 atm, $CH_4/CO_2 = 1$, T = 650 °C, $WHSV = 30\ L.g^{-1}.h^{-1}$.

can be predicted by the lack of active metallic phase in the solid. The 2% doped catalyst, LNZ2, is comparatively inactive despite its metal loading. Samples doped with loadings greater than 2% have been found to be active for DRM. Interestingly this also corresponds to the loading limit for which a secondary perovskite phase has been formed. However, despite an initial conversion of 33% for CO_2 and 18% for CH_4, LNZ5 is rapidly deactivated and its activity reaches a plateau at 17% for CO_2 and 6.6% for CH_4 after 20 h on stream. On the other hand, the 10% doped catalyst displays very good performance in terms of both catalytic activity and stability. LNZ10 achieves a conversion of 79% for CO_2 and 65% for CH_4 and reaches steady state in less than 1 h. No deactivation is observed after 30 h on stream.

3.2.1. Temperature effect

The dependence of the activity of the 10% Ni doped catalyst with the reaction temperature was further studied. Fig. 5 illustrates the catalytic activity of the best catalyst, LNZ10, over temperatures ranging from 600 to 700 °C, each point corresponding to the steady state value after 30 h on stream. Higher temperatures were also studied at high space velocities and the results are shown in Fig. S1 (Supporting information) showing excellent conversion levels at temperature beyond 800 °C. LNZ10 is found to be very active, even at low temperature, with CH_4 and CO_2 conversions of 53% and 69% respectively at 600 °C. Moreover, LNZ10 did not deactivate and showed a stable behaviour for
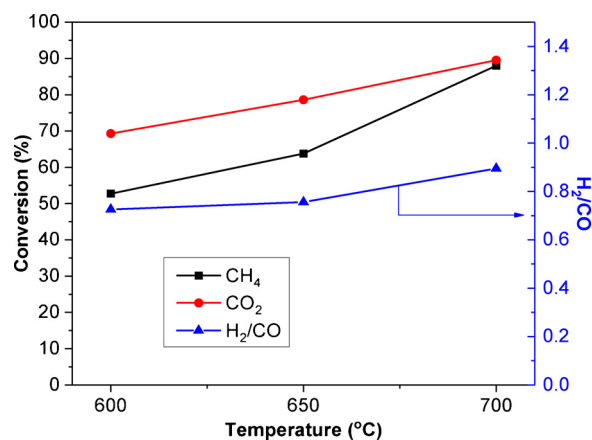

Fig. 5. Effect of the temperature on H_2/CO ratio and CH_4 and CO_2 conversion for LNZ10. Reaction conditions: P = 1 atm, $CH_4/CO_2 = 1$, $WHSV = 30\ L.g^{-1}.h^{-1}$.

30 h on stream at this low temperature for DRM, where carbon formation is thermodynamically favoured, emphasising its great resistance to carbon formation. In accordance with thermodynamic equilibrium calculations, both conversions increased with temperature. Remarkably, as temperature increased the gap between CO_2 conversion and CH_4 conversion decreased until both conversions became equal at 700 °C. Indeed, methane conversion is believed to be favoured at high temperature due to the high activation energy of CH_4. A slight increase of the H_2/CO ratio is observed as temperature increases, which is due to a higher CH_4 conversion leading to greater H_2 production. Although the syngas trend is affected also by the parallel reactions as for example methane decomposition (eq. 3) and RWGS (eq. 6) both leading to opposite effects – RWGS consumes H_2 while CH_4 decomposition generates extra H_2. In fact, among the parallel reactions affecting DRM, the RWGS has a remarkable influence in the reactant conversions and H_2/CO ratio as previously observed in literature [44,45].

3.2.2. Space velocity effect

Space velocity is a key parameter for industrial applications, as it determines the volume of the reforming unit and therefore is directly linked to the capital cost of the process. The 10% doped catalyst was tested utilising different Weight Hourly Space Velocities (WHSV). For this test, the mass of catalyst was kept constant and the flow of reactant was halved and doubled to give WHSVs of 15, 30 and 60 $L.g^{-1}.h^{-1}$. Experiments were conducted at 700 °C for 30 h. Once again, the catalyst showed great stability even at low space velocity, showing no sign of deactivation and therefore testifying of the outstanding resistance to coking of this catalyst even when exposed to hard conditions. Fig. 6 illustrates the behaviour of the LNZ10 catalyst in terms of CH_4 conversion, CO_2 conversion and H_2/CO ratio as functions of the space velocity, considering the steady state values.

At low space velocities the catalyst achieves very high conversions: 88% for CH_4 and 91% for CO_2 at 15 $L.g^{-1}.h^{-1}$. A slight decrease in CH_4 conversion is observed when increasing the space velocity to 30 $L.g^{-1}.h^{-1}$. When doubling the space velocity to 60 $L.g^{-1}.h^{-1}$ a drop in activity is witnessed; however the conversions obtained are still relatively good especially for CO_2 (74.5%). Methane conversion decreased by a greater extent to 55.5% due once again to the difficulty in overcoming CH_4 activation since its C−H bonds are very stable.

Overall, the temperature effect and the space velocity tests reveal the excellent performance of our engineered catalyst under a variety of reaction conditions. The relatively good behaviour at 600 °C suggests that this catalyst can be envisaged as suitable low temperature DRM catalyst (overcoming the coking limitations imposed by
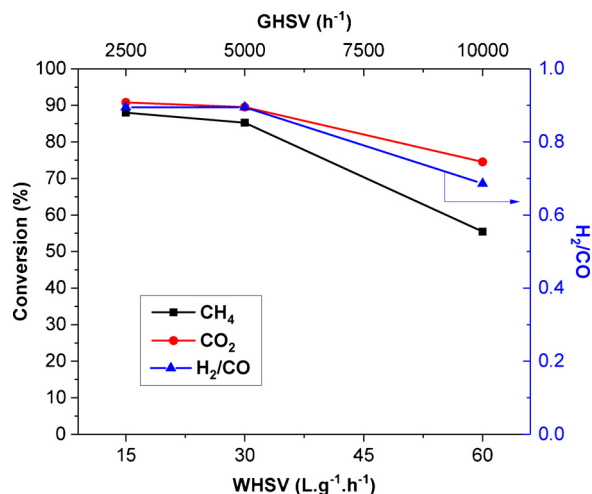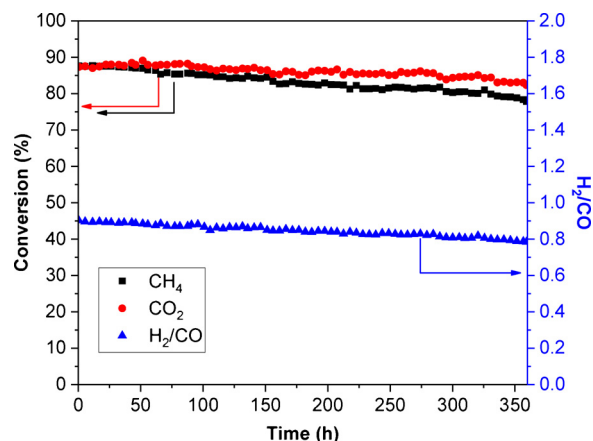

Fig. 7. Stability test on LNZ10 over 360 h. Reaction conditions: CH_4/CO_2:1, P = 1 atm, T = 700 °C and WHSV = 30 $L.g^{-1}.h^{-1}$.

thermodynamics). Also its high activity at relatively demanding space velocity conditions indicates its potential applications in compact units (i.e. direct biogas solid oxide fuel cells, or medium size reformers for syngas generation).

3.2.3. Stability test

A stability test was conducted to check the behaviour of the 10% Ni-doped pyrochlore over a period of two weeks, the results of which are shown in Fig. 7. The catalyst displayed great stability over time on stream but showed signs of small deactivation starting with CH_4 and CO_2 conversions of 87% and attaining conversions of 82% and 77.8% for CO_2 and CH_4 respectively, after 360 h on stream. This corresponds to a declination rate of 0.0138% h^{-1} for CO_2 and 0.0255% h^{-1} for CH_4. Methane conversion appears to be more sensitive to deactivation than CO_2. Deactivation in our case is due to carbon formation around or over the Ni particles, as revealed by TEM (Fig. 10) since methane is believed to be activated by Ni [46]. In this situation it is understandable that CH_4 conversion is more affected than CO_2. In fact, as reported by Verykios et al. in a DRM study over Ni supported on La_2O_3, CO_2 is activated by the support [47]. It is assumed in our case that CO_2 is activated on the La-O phase of the pyrochlore, forming lanthanum oxycarbonates ($La_2O_2CO_3$) that are then reduced to CO [26].

Nevertheless, despite the reaction and deactivation mechanisms, LNZ10 has demonstrated excellent stability since it is able to maintain outstanding levels of CO_2/CH_4 conversions in continuous operation over a period of two weeks producing good quality syngas. A comparison time on stream test with a standard ceria promoted Ni/Al_2O_3 catalyst is provided in Fig. S2, emphasizing the excellent stability of the

Fig. 6. Effect of the space velocity on H_2/CO ratio and CH_4 and CO_2 conversion for LNZ10. Reaction conditions: P = 1 atm, CH_4/CO_2 = 1, T = 700 °C.
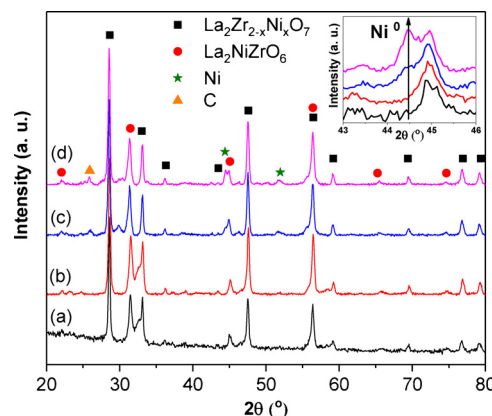

Fig. 8. XRD patterns of LNZ10: (a) calcined, (b) reduced, (c) after 30 h reaction and (d) after 360 h reaction.

pyrochlore catalyst.

3.3. Post reaction characterisation

All the prepared catalysts were analysed post reaction using XRD to detect any structural changes after the different treatments they underwent. Fig. 8 shows the XRD patterns of the 10% Ni pyrochlore-based catalyst as prepared, after reduction under hydrogen at 700 °C for 1 h, after DRM reaction at 650 °C for 30 h and after DRM reaction at 700 °C for 360 h. No differences in the diffraction patterns were observed between the 'as prepared' or 'post reaction' for catalysts with less than 10% Ni loading (not shown). This indicates that neither the pre-treatment under hydrogen nor the reaction conditions affected the crystallinity of the materials revealing the high thermal stability of Ni-doped pyrochlores. On the other hand, small changes can be observed on the 10% Ni catalyst. Although the pyrochlore phase and the perovskite phase remain intact, small peaks centred at 2θ = 44.4° and 51.7°, corresponding to the characteristic (111) and (200) planes of the metallic Ni phase, appear on the XRD profiles of LNZ10 after reaction, first as a shoulder peak after 30 h of reaction and then as a distinguished peak after 360 h of reaction as shown in the inset of Fig. 8. This suggests the progressive exsolution of Ni from the pyrochlore to the surface of the catalyst during the reaction. In fact, we have previously shown (Fig. 3) that TPR indicates that some bulk NiO is present on the surface of LNZ5 and LNZ10, which is reduced to Ni°. No Ni° peaks are detected on the XRD profiles of the reduced catalysts suggesting that the Ni particles on the surface of the pyrochlore cannot be detected and are small (< 5 nm) and well dispersed. Growth of the Ni crystallite size was estimated using the Scherrer equation. After 30 h of reaction the Ni particle size is about 20 nm while after 360 h on stream the particle size is ca. 26 nm. This small change emphasizes the robustness of LNZ10 and shows how the substitution of Ni inside a complex oxide structure actually prevents sintering of the metal particles. In any case it seems that our catalytic active phase is composed by small Ni clusters dispersed on the catalyst surface along with well dispersed Ni particles exsolved from the pyrochlore lattice. As reported by Kwon et al., exsolution of transition metals is a smart catalyst design approach for energy applications in particular when the metal has a good ability to exsolve under a reducing or reaction environments [48].

Although, the exsolution strategy successfully mitigates Ni particles agglomeration, carbon formation over Ni clusters is hard to avoid. In fact, carbon formation is not always detrimental and in a way is an indication of the catalytic activity, since C−H activation of CH_4 involves the formation of C* species reported in many computational studies [49,50]. In our case, a small amount of graphitic carbon is detected on the spent LNZ10 sample, with the appearance of a peak at ~ 26°. This peak corresponds to the graphite lattice plane (002) of carbon nanotubes [51].

The catalysts were recovered after being tested under DRM conditions and further characterised. A combined TPO-TGA, TEM and Raman spectroscopy study (see Fig. S3 in the supporting information for the Raman data) was used to quantify and identify the carbonaceous species formed on the catalysts and responsible for their deactivation. Fig. 9 shows the CO_2 production profiles of LNZ10 after 30 h reaction at different temperatures and after the stability test, in the temperature-programmed oxidation experiment. LZ and LNZ2 do not contain any carbon as they were not active for DRM, in good agreement with DFT studies and the discussion mentioned above. Carbon formation is a sign of activity in DRM; the key point is to avoid the formation of hard carbon deposits. The profile of LNZ5 (not shown) indicates the presence of traces of carbonaceous species which are oxidised at 500 and 700 °C in accordance with the relatively low activity that it presented. LNZ10 on the other hand, contains a larger amount of carbon, with one major TPO peak at 520 °C. This peak corresponds to a soft type of carbon since it can be oxidised under relatively mild conditions. Carbon deposition is closely related to Ni particle size, the larger the clusters the more
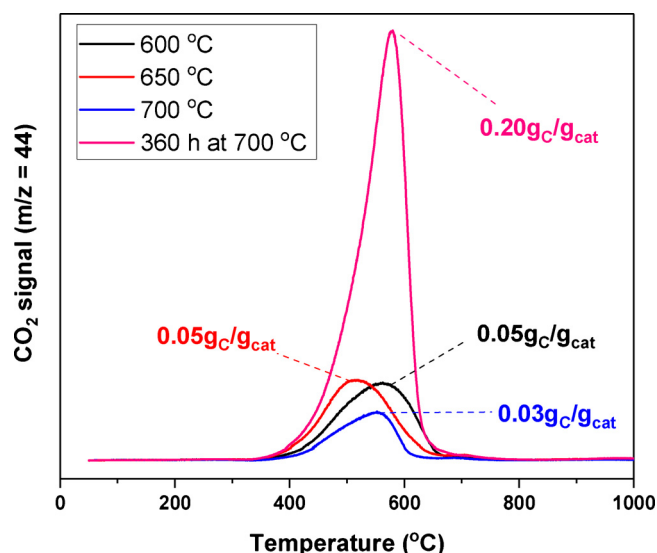

Fig. 9. TPO profiles of LNZ10 after DRM during 30 h at different temperatures and after 360 h at 700 °C.

favoured the carbon formation [52–55]. The fact that soft carbon is present also supports the exsolution hypothesis leading to small Ni domains available at the catalyst surface during reaction. The agglomeration of Ni clusters would lead to more graphitic carbon, therefore the Ni particles of our catalyst seem to remain small and well dispersed on the surface.

The reaction temperature has an important influence on carbon deposition. Whether reacting at 600 or 650 °C a similar amount of carbonaceous species seems to be formed (0.05 g_C/g_{cat}). However, upon reaction at 700 °C a decrease in carbon formation is observed (0.03 g_C/g_{cat}). This is in accordance with the thermodynamic equilibrium showing that carbon formation is favoured at low temperatures. As expected after 360 h on stream, relatively high quantities of carbon have been formed on the catalyst (0.20 g_C/g_{cat}), however, the performance of the catalyst was only slightly affected.

Further insights of carbon deposition was obtained by electronic microscopy. TEM images of LNZ10 (a) reduced, (b) after 30 h of reaction, (c) and (d) after 360 h of reaction are shown in Fig. 10. Image (a) shows that Ni is mainly present in the bulk of the catalyst. After 30 h of reaction some carbon nanotubes (CNTs) are formed and after 360 h of reaction a significant amount of CNTs are found. The wall thickness of the nanotubes (11 nm) indicates multi-wall CNTs. Interestingly, the growth of CNTs starts from the interface between the metallic particle and the catalyst bulk and separates nickel from the surface as they grow. As reported previously, carbon nano-fibres tend to cover Ni particles causing the deactivation of the catalyst, but in the case of carbon nanotubes, Ni particles can be located on the tip of the CNTs or at the base, and may still catalyse methane decomposition [55,56]. In our case, CNTs grow away from the catalyst particle through a reversal growth behaviour as previously observed by Titus et al. [10] rather than covering the surface. This growing mechanism allows part of the catalyst particles to remain accessible and the active sites to function (as shown on Fig. 10(c,d)). In other words, despite the unavoidable carbon formation, our Ni-stabilised catalyst remains active simply because carbon is covering just a small fraction of the active sites and most of the Ni atoms (in the pyrochlore-perovskite phase or exsolved in the surface) are available for the reaction leading to the outstanding long-term stability.

4. Conclusions

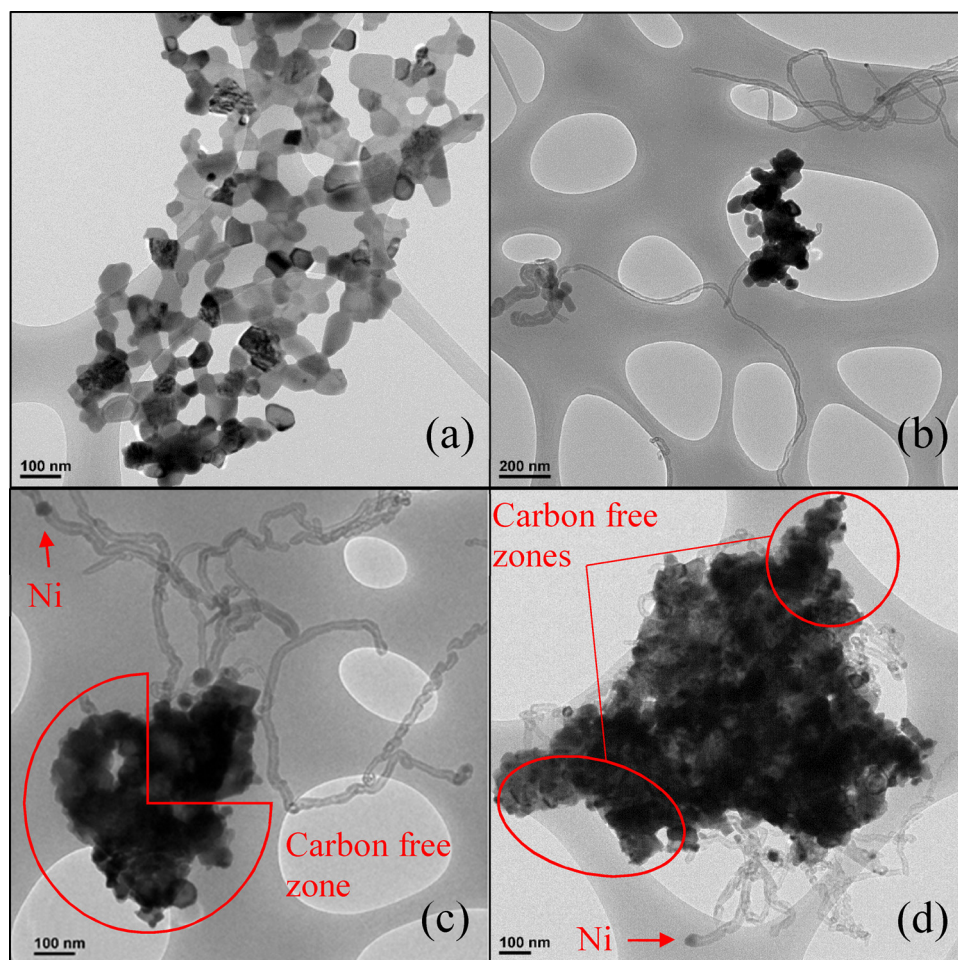A novel series of advanced nickel-based catalysts was prepared,

Fig. 10. TEM images of LNZ10: (a) reduced, (b) after 30 h of reaction, (c) and (d) after 360 h of reaction at 700 °C.

characterised and tested for DRM. Nickel was stabilised within a thermally stable mixed oxide structure, to prevent Ni from sintering and therefore from forming large clusters that favors carbon formation. $La_2Zr_2O_7$ pyrochlore was selected and doped with different Ni loadings. XRD and Raman analysis of the calcined samples confirmed the formation of the pyrochlore phase as well as Ni substitution in the pyrochlore. The 5 and 10% Ni doped pyrochlore were found to be active for DRM and presented an additional perovskite phase. LNZ5 deactivated quickly whereas LNZ10 displayed outstanding catalytic activity and stability over a long term stability test of 360 h. TPO and TEM analysis were performed on the spent catalysts and multiwall carbon nanotubes were identified as being formed on the surface. However, this had a limited impact on the catalyst's activity proving the robustness of the 10% doped pyrochlore. Structural analysis was conducted on the catalyst after 360 h of reaction using XRD, and reveals that the pyrochlore structure remains intact during reaction and that Ni was exsolved to the surface during reaction generating small Ni clusters which are responsible for the observed high activity.

Overall, this work presents a strategy to design economically viable catalysts able to withstand the demanding conditions of dry reforming processes. The successful results obtained with our Ni-stabilized materials suggest their potential application for biogas upgrading, flexible syngas production and CO_2 cleaning up processes.

Acknowledgments

Appendix A. Supplementary data

Supplementary material related to this article can be found, in the online version, at doi:https://doi.org/10.1016/j.apcatb.2018.05.051.

References

[1] L.A. Schulz, L.C.S. Kahle, K.H. Delgado, S.A. Schunk, A. Jentys, O. Deutschmann, J.A. Lercher, On the coke deposition in dry reforming of methane at elevated pressures, Appl. Catal. A 504 (2015) 599–607.

[2] D. Pakhare, J. Spivey, A review of dry (CO_2) reforming of methane over noble metal catalysts, Chem. Soc. Rev. 43 (2014) 7813–7837.

[3] A. Wolfbeisser, O. Sophiphun, J. Bernardi, J. Wittayakun, K. Föttinger, G. Rupprechter, Methane dry reforming over ceria-zirconia supported Ni catalysts, Catal. Today 277 (2016) 234–245.

[4] R. Chai, G. Zhao, Z. Zhang, P. Chen, Y. Liu, Y. Lu, High sintering-/coke-resistance Ni@SiO$_2$/Al$_2$O$_3$/FeCrAl-fiber catalyst for dry reforming of methane: one-step, macro-to-nano organization via cross-linking molecules, Catal. Sci. Technol. 7 (2017) 5500–5504.

[5] M.K. Nikoo, N.A.S. Amin, Thermodynamic analysis of carbon dioxide reforming of methane in view of solid carbon formation, Fuel Process. Technol. 92 (2011) 678–691.

[6] P. Boldrin, E. Ruiz-Trejo, J. Mermelstein, J.M. Bermúdez Menéndez, T. Ramírez Reina, N.P. Brandon, Strategies for carbon and sulfur tolerant solid oxide fuel cell materials, incorporating lessons from heterogeneous catalysis, Chem. Rev. 116 (2016) 13633–13684.

[7] J.-M. Lavoie, Review on dry reforming of methane, a potentially more environmentally-friendly approach to the increasing natural gas explosion, Front.

Chem. 2 (2014).

[8] M. Muraleedharan Nair, S. Kaliaguine, Structured catalysts for dry reforming of methane, New J. Chem. 40 (2016) 4049–4060.

[9] L. Zhang, Q. Zhang, Y. Liu, Y. Zhang, Dry reforming of methane over Ni/MgO-Al₂O₃ catalysts prepared by two-step hydrothermal method, Appl. Surf. Sci. 389 (2016) 25–33.

[10] J. Titus, T. Roussière, G. Wasserschaff, S. Schunk, A. Milanov, E. Schwab, G. Wagner, O. Oeckler, R. Gläser, Dry reforming of methane with carbon dioxide over NiO–MgO–ZrO₂, Catal. Today 270 (2016) 68–75.

[11] B. Abdullah, N.A. Abd Ghani, D.-V.N. Vo, Recent advances in dry reforming of methane over Ni-based catalysts, J. Clean. Prod. 162 (2017) 170–185.

[12] C.-j. Liu, J. Ye, J. Jiang, Y. Pan, Progresses in the preparation of coke resistant Ni-based catalyst for steam and CO₂ reforming of methane, ChemCatChem 3 (2011) 529–541.

[13] J.J. Spivey, Deactivation of reforming catalysts, in: J.J.S. Dushyant Shekhawat, David A Berry (Eds.), Fuel Cells: Technologies for Fuel Processing, Elsevier, Oxford, UK, 2011pp. 285–315.

[14] O. Muraza, A. Galadima, A review on coke management during dry reforming of methane, Int. J. Energy Res. 39 (2015) 1196–1216.

[15] S.M. de Lima, J.M. Assaf, Synthesis and characterization of LaNiO₃, LaNi(1-x)FeₓO₃ and LaNi(1-x)CoₓO₃ perovskite oxides for catalysis application, Mater. Res. 5 (2002) 329–335.

[16] S. Dama, S.R. Ghodke, R. Bobade, H.R. Gurav, S. Chilukuri, Active and durable alkaline earth metal substituted perovskite catalysts for dry reforming of methane, Appl. Catal. B 224 (2018) 146–158.

[17] X. Zhang, X. Fang, X. Feng, X. Li, W. Liu, X. Xu, N. Zhang, Z. Gao, X. Wang, W. Zhou, Ni/Ln₂Zr₂O₇ (Ln = La, Pr, Sm and Y) catalysts for methane steam reforming: the effects of A site replacement, Catal. Sci. Technol. 7 (2017) 2729–2743.

[18] Y. Ma, X. Wang, X. You, J. Liu, J. Tian, X. Xu, H. Peng, W. Liu, C. Li, W. Zhou, P. Yuan, X. Chen, Nickel-supported on La₂Sn₂O₇ and La₂Zr₂O₇ pyrochlores for methane steam reforming: insight into the difference between Tin and Zirconium in the B site of the compound, ChemCatChem 6 (2014) 3366–3376.

[19] J.M. Sohn, M.R. Kim, S.I. Woo, The catalytic activity and surface characterization of Ln₂B₂O₇ (Ln = Sm, Eu, Gd and Tb; B = Ti or Zr) with pyrochlore structure as novel CH₄ combustion catalyst, Catal. Today 83 (2003) 289–297.

[20] J.L. Rogers, M.C. Mangarella, A.D. D'Amico, J.R. Gallagher, M.R. Dutzer, E. Stavitski, J.T. Miller, C. Sievers, Differences in the nature of active sites for methane dry reforming and methane steam reforming over nickel aluminate catalysts, ACS Catal. 6 (2016) 5873–5886.

[21] J. Titus, M. Goepel, S.A. Schunk, N. Wilde, R. Gläser, The role of acid/base properties in Ni/MgO-ZrO₂–based catalysts for dry reforming of methane, Catal. Commun. 100 (2017) 76–80.

[22] X. Fang, X. Zhang, Y. Guo, M. Chen, W. Liu, X. Xu, H. Peng, Z. Gao, X. Wang, C. Li, Highly active and stable Ni/Y₂Zr₂O₇ catalysts for methane steam reforming: on the nature and effective preparation method of the pyrochlore support, Int. J. Hydrogen Energy 41 (2016) 11141–11153.

[23] R. Kieffer, M. Fujiwara, L. Udron, Y. Souma, Hydrogenation of CO and CO₂ toward methanol, alcohols and hydrocarbons on promoted copper-rare earth oxides catalysts, Catal. Today 36 (1997) 15–24.

[24] S.-F. Weng, Y.-H. Wang, C.-S. Lee, Autothermal steam reforming of ethanol over La₂Ce₂₋ₓRuₓO₇ (x = 0–0.35) catalyst for hydrogen production, Appl. Catal. B 134–135 (2013) 359–366.

[25] S.-F. Weng, H.-C. Hsieh, C.-S. Lee, Hydrogen production from oxidative steam reforming of ethanol on nickel-substituted pyrochlore phase catalysts, Int. J. Hydrogen Energy 42 (2017) 2849–2860.

[26] D. Pakhare, C. Shaw, D. Haynes, D. Shekhawat, J. Spivey, Effect of reaction temperature on activity of Pt- and Ru-substituted lanthanum zirconate pyrochlores (La₂Zr₂O₇) for dry (CO₂) reforming of methane (DRM), J. CO2 Util. 1 (2013) 37–42.

[27] D. Pakhare, H. Wu, S. Narendra, V. Abdelsayed, D. Haynes, D. Shekhawat, D. Berry, J. Spivey, Characterization and activity study of the Rh-substituted pyrochlores for CO₂ (dry) reforming of CH₄, Appl. Petrochem. Res. 3 (2013) 117–129.

[28] D. Pakhare, D. Haynes, D. Shekhawat, J. Spivey, Role of metal substitution in lanthanum zirconate pyrochlores (La₂Zr₂O₇) for dry (CO2) reforming of methane (DRM), Appl. Petrochem. Res. 2 (2012) 27–35.

[29] S. Gaur, D. Pakhare, H. Wu, D.J. Haynes, J.J. Spivey, CO₂ reforming of CH₄ over Ru-substituted pyrochlore catalysts: effects of temperature and reactant feed ratio, Energy Fuels 26 (2012) 1989–1998.

[30] S. Gaur, D.J. Haynes, J.J. Spivey, Rh, Ni, and Ca substituted pyrochlore catalysts for dry reforming of methane, Appl. Catal. A 403 (2011) 142–151.

[31] N. Kumar, Z. Wang, S. Kanitkar, J.J. Spivey, Methane reforming over Ni-based pyrochlore catalyst: deactivation studies for different reactions, Appl. Petrochem. Res. 6 (2016) 201–207.

[32] T.R. Reina, E. le Saché, D. Watson, L. Pastor Perez, A. Sepulveda Escribano, Catalysts for the reforming of gaseous mixtures, GB1704017.1 (2017).

[33] T. Stroud, T.J. Smith, E. Le Saché, J.L. Santos, M.A. Centeno, H. Arellano-Garcia, J.A. Odriozola, T.R. Reina, Chemical CO₂ recycling via dry and bi reforming of methane using Ni-Sn/Al₂O₃ and Ni-Sn/CeO₂-Al₂O₃ catalysts, Appl. Catal. B 224 (2018) 125–135.

[34] C. Wan, W. Zhang, Y. Wang, Z. Qu, A. Du, R. Wu, W. Pan, Glass-like thermal conductivity in ytterbium-doped lanthanum zirconate pyrochlore, Acta Mater. 58 (2010) 6166–6172.

[35] H. Chen, Y. Gao, Y. Liu, H. Luo, Coprecipitation synthesis and thermal conductivity of La₂Zr₂O₇, J. Alloys Compd. 480 (2009) 843–848.

[36] K. Holliday, S. Finkeldei, S. Neumeier, C. Walther, D. Bosbach, T. Stumpf, TRLFS of Eu³⁺ and Cm³⁺ doped La₂Zr₂O₇: a comparison of defect fluorite to pyrochlore structures, J. Nucl. Mater. 433 (2013) 479–485.

[37] D.J. Haynes, D.A. Berry, D. Shekhawat, J.J. Spivey, Catalytic partial oxidation of n-tetradecane using pyrochlores: effect of Rh and Sr substitution, Catal. Today 136 (2008) 206–213.

[38] D.J. Haynes, D. Shekhawat, D.A. Berry, J. Zondlo, A. Roy, J.J. Spivey, Characterization of calcination temperature on a Ni-substituted lanthanum-strontium-zirconate pyrochlore, Ceram. Int. 43 (2017) 16744–16752.

[39] L. Kong, I. Karatchevtseva, D.J. Gregg, M.G. Blackford, R. Holmes, G. Triani, A novel chemical route to prepare La₂Zr₂O₇ pyrochlore, J. Am. Ceram. Soc. 96 (2013) 935–941.

[40] S. Wang, W. Li, S. Wang, Z. Chen, Synthesis of mesoporous La₂Zr₂O₇ with high surface area by combining epoxide-mediated sol-gel process and solvothermal treatment, Microporous Mesoporous Mater. 234 (2016) 137–145.

[41] M.T. Vandenborre, E. Husson, Comparison of the force field in various pyrochlore families. I. The A₂B₂O₇ oxides, J. Solid State Chem. 50 (1983) 362–371.

[42] D. Michel, M. Perez y Jorba, R. Collongues, Study by Raman spectroscopy of order-disorder phenomena occurring in some binary oxides with fluorite-related structures, J. Raman Spectrosc. 5 (1976) 163–180.

[43] M. Pokhrel, M. Alcoutlabi, Y. Mao, Optical and X-ray induced luminescence from Eu³⁺ doped La₂Zr₂O₇ nanoparticles, J. Alloys Compd. 693 (2017) 719–729.

[44] M.C.J. Bradford, M.A. Vannice, CO₂ reforming of CH₄, Catal. Rev. 41 (1999) 1–42.

[45] E. le Saché, J.L. Santos, T.J. Smith, M.A. Centeno, H. Arellano-Garcia, J.A. Odriozola, T.R. Reina, Multicomponent Ni-CeO₂ nanocatalysts for syngas production from CO₂/CH₄ mixtures, J. CO2 Util. 25 (2018) 68–78.

[46] A. Slagtern, Y. Schuurman, C. Leclercq, X. Verykios, C. Mirodatos, Specific features concerning the mechanism of methane reforming by carbon dioxide over Ni/La₂O₃Catalyst, J. Catal. 172 (1997) 118–126.

[47] X.E. Verykios, Catalytic dry reforming of natural gas for the production of chemicals and hydrogen, Int. J. Hydrogen Energy 28 (2003) 1045–1063.

[48] O. Kwon, S. Sengodan, K. Kim, G. Kim, H.Y. Jeong, J. Shin, Y.-W. Ju, J.W. Han, G. Kim, Exsolution trends and co-segregation aspects of self-grown catalyst nanoparticles in perovskites, Nat. Commun. 8 (2017) 15967.

[49] Y.-A. Zhu, D. Chen, X.-G. Zhou, W.-K. Yuan, DFT studies of dry reforming of methane on Ni catalyst, Catal. Today 148 (2009) 260–267.

[50] F. Polo-Garzon, M. He, D.A. Bruce, Ab initio derived reaction mechanism for the dry reforming of methane on Rh doped pyrochlore catalysts, J. Catal. 333 (2016) 59–70.

[51] A.S. Ferlauto, D.Z. de Florio, F.C. Fonseca, V. Esposito, R. Muccillo, E. Traversa, L.O. Ladeira, Chemical vapor deposition of multi-walled carbon nanotubes from nickel/yttria-stabilized zirconia catalysts, Appl. Phys. A 84 (2006) 271–276.

[52] J.R. Rostrup-Nielsen, Sulfur-passivated nickel catalysts for carbon-free steam reforming of methane, J. Catal. 85 (1984) 31–43.

[53] S. Damyanova, B. Pawelec, K. Arishtirova, J.L.G. Fierro, C. Sener, T. Dogu, MCM-41 supported PdNi catalysts for dry reforming of methane, Appl. Catal. B 92 (2009) 250–261.

[54] R. Yang, C. Xing, C. Lv, L. Shi, N. Tsubaki, Promotional effect of La₂O₃ and CeO₂ on Ni/γ-Al₂O₃ catalysts for CO₂ reforming of CH₄, Appl. Catal. A 385 (2010) 92–100.

[55] M.H. Amin, K. Mantri, J. Newnham, J. Tardio, S.K. Bhargava, Highly stable ytterbium promoted Ni/γ-Al₂O₃ catalysts for carbon dioxide reforming of methane, Appl. Catal. B 119 (2012) 217–226.

[56] L. Zhou, L. Li, N. Wei, J. Li, J.-M. Basset, Effect of NiAl₂O₄ formation on Ni/Al₂O₃ stability during dry reforming of methane, ChemCatChem 7 (2015) 2508–2516.